Nuclear Instruments and Methods in Physics Research B 326 (2014) 243–246

Contents lists available at ScienceDirect

Nuclear Instruments and Methods in Physics Research B

journal homepage: www.elsevier.com/locate/nimb

Radiation defects in complex perovskite solid solutions

M.M. Kuklja [a,*], E.A. Kotomin [b,c], O. Sharia [a], Yu.A. Mastrikov [a,b], J. Maier [c]

[a] Materials Science and Engineering Dept., University of Maryland, College Park, USA
[b] Institute for Solid State Physics, University of Latvia, Riga, Latvia
[c] Max Planck Institute for Solid State Research, Heisenbergstr. 1, 70569 Stuttgart, Germany

ARTICLE INFO

Article history:
Received 1 July 2013
Received in revised form 28 August 2013
Accepted 30 August 2013
Available online 24 January 2014

Keywords:
Solid solutions
First principles calculations
Frenkel and Schottky disorder
Clustering effect
Antisite defects

ABSTRACT

First principles density functional theory (DFT) based modeling is performed to explore formation energies of a series of point cation and oxygen defects, Frenkel and Schottky disorder, as well as structural disorder in $Ba_{1-x}Sr_xCo_{1-y}Fe_yO_{3-\delta}$ (BSCF) perovskite solid solutions. The results are compared with previous studies on a prototype $SrTiO_3$ perovskite. It is shown that BSCF permits accommodation of a high concentration of defects and cation clusters but not antisite defects.

Published by Elsevier B.V.

1. Introduction

Two ABO_3-type perovskite solid solutions (BSCF: $Ba_{1-x}Sr_xCo_{1-y}Fe_yO_{3-\delta}$ and LSCF: $La_{1-x}Sr_xCo_{1-y}Fe_yO_{3-\delta}$), mixed ionic–electronic conductors, have attracted a lot of attention because of a range of potential applications in progressive technologies, gas separation membranes, solid oxide fuel cells (SOFC) [1], and others. The use of SOFC for electricity supply in space stations raises a question of radiation stability of these materials. Clearly, radiation defects, first of all, vacancies and antisite defects in perovskites, would affect many properties and performance of these materials in targeted applications. In recent reports [2–4], we performed first principles studies of formation energies of oxygen vacancies in BSCF and demonstrated that oxygen vacancies require much smaller energies than those in simple perovskites, e.g. $SrTiO_3$ or $LaMnO_3$. It was suggested that this fact explains considerable non-stoichiometry in oxygen observed in BSCF. With respect to more complex defects, we are familiar only with a study of Frenkel defects in $SrTiO_3$ [5], which was performed using both interatomic potentials and DFT method. In this paper, we discuss results of first principles DFT calculations of point cation and oxygen defects, Frenkel and Schottky defects, as well as structural disorders in complex perovskites.

2. Details of calculations

This research is performed by means of density functional theory (DFT) as implemented in the computer code VASP 4.6 [6] with Projector Augmented Wave (PAW) pseudopotentials and the exchange–correlation GGA functional of the PBE-type. We used the soft PAW PBE potential for O ions, which yields a binding energy for a free O_2 molecule very close to the experimental value and a reasonable O–O bond length (5.24 eV and 1.29 Å, cf. the experimental values of 5.12 eV and 1.21 Å, respectively [7]). All $ABO_{3-\delta}$ cubic perovskites (both oxygen-stoichiometric, $\delta = 0$, as well as oxygen-deficient, $\delta > 0$) were simulated using large periodic supercells that were constructed by expanding the five-atom ABO_3-type cubic primitive unit cell by $2 \times 2 \times 2$ (40 atoms) and by $4 \times 4 \times 4$ (320 atoms). The $8 \times 8 \times 8$ k-point mesh was created using the Monkhorst–Pack scheme [8] for the ABO_3 unit cell, $4 \times 4 \times 4$ mesh used for 40 atom supercells and $2 \times 2 \times 2$ for 320 atom supercells to keep the density of k-point mesh consistent. The largest, 320 atom supercells were used for modeling pairs of Frenkel defects as they allow to accommodate both the close and the distant pairs in the same supercells, and for modeling of the antisite defects. Ionic charges were calculated by the Bader method [9]. The kinetic energy cut-off for the plane wave basis set was set to 520 eV. The basic properties of defect-free BSCF and of oxygen vacancies therein were detailed in our previous publications [2–4]. In the calculations reported here, the most common in experiments material composition $Ba_{0.5}Sr_{0.5}Co_{0.75}Fe_{0.25}O_3$ was modeled, unless indicated otherwise. Note that in vacancy calculations, a whole supercell is neutral, the charge redistribution around a vacancy is calculated self-consistently according to the minimum of the total energy [3,4]. Thus, there is no need to take into account interactions of the charged defects in periodic cells.

* Corresponding author. Tel.: +1 7032924940.
E-mail addresses: mkukla@nsf.gov, mkukla@umd.edu (M.M. Kuklja).

0168-583X/$ - see front matter Published by Elsevier B.V.
http://dx.doi.org/10.1016/j.nimb.2013.08.068

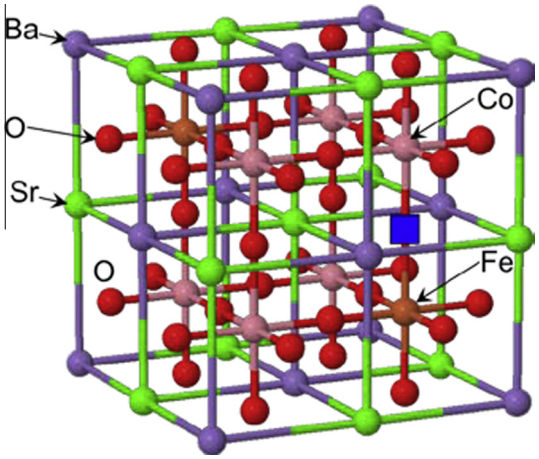

Fig. 1. A single oxygen vacancy (a blue square) is shown in the model BSCF supercell. (For interpretation of the references to color in this figure legend, the reader is referred to the web version of this article.)

3. Single vacancies and Schottky disorder

The cation vacancy formation energy E_V was calculated from the reaction:

$$Me^{x}_{Me} \longrightarrow V^{y}_{Me} + Me_{(g)} \quad (1)$$

where Me = Ba, Sr, Co, or Fe, and $y = 2$ for A-site cations, Ba and Sr, and $y = 4$ for B-site cations, Co and Fe, and an index (g) indicates that the metal left the crystal as an isolated atom. The oxygen vacancy (Fig. 1) formation energy E_V was calculated from the equation:

$$O^{x}_{O} + 2M^{x}_{M} \longrightarrow \frac{1}{2}O_2 + V^{\cdot\cdot}_{O} + 2M'_{M} \quad (2a)$$

and includes a decrease of the oxidation state of two transition metal atoms due to two electrons left behind by the removed oxygen [4]. Due to equilibrium between electrons and holes, this equation can be rewritten in terms of holes rather than electrons:

$$O^{x}_{O} + 2M^{\cdot}_{M} \longrightarrow \frac{1}{2}O_2 + V^{\cdot\cdot}_{O} + 2M^{x}_{M} \quad (2b)$$

Table 1 shows that the oxygen vacancy formation requires a considerably smaller energy E_V (~4 eV) than cation vacancies (8.6–9.3 eV), all obtained with respect to isolated atoms. The oxygen vacancy formation energy calculated with respect to 1/2 free O_2 molecule in the triplet state yields 1.34 eV for the oxygen vacancy placed between two Co atoms (Co–O–Co) and 1.40 eV between one Co and one Fe atom (Co–O–Fe) [3]. These energies are significantly smaller than those for a wide-gap perovskite $SrTiO_3$ (ca. 6 eV) [10] and even for $La_{0.75}Sr_{0.25}MnO_3$ used in SOFC applications (2.7 eV) [11,12]. Under normal, oxygen-rich conditions, the oxygen vacancy formation energy shows a strong temperature- and gas-pressure dependence as recently analyzed [12].

The energy of full Schottky disorder is derived from the equation:

$$0_{(bulk \rightarrow surface)} \leftrightarrow 2V''_{Ba} + 2V''_{Sr} + 3V''''_{Co} + V''''_{Fe} + 12V^{\cdot\cdot}_{O} \quad (3)$$

The left-hand side represents the total energy of an ideal 40 atom (8 formula units) BSCF supercell. The right-hand side describes a set of vacancies, with each individual vacancy placed in a separate 40 atom BSCF supercell. The energy of the right-hand side is normalized per defect to make it comparable to different equations implied in Table 1. The simulated Schottky disorder requires 0.90 eV per defect. This energy is low and indicates that the vacancy disorder is favored in BSCF perovskites.

4. Frenkel disorder

Among Frenkel defects explored in BSCF, the oxygen vacancy-interstitial pairs have the lowest energy of ~0.75–0.89 eV per defect (Table 1). This is in agreement with the low formation energies of the respective single oxygen vacancies [2–4].

We found that the formation energies for oxygen Frenkel defects in BSCF turned out to be much smaller than those in other perovskites, e.g. $SrTiO_3$ (~10 eV) [5], which translates into a much higher equilibrium concentration of defects. Both the *split* and *hollow* configurations were probed for interstitial atoms (Fig. 2) for close (~5 Å) and distant (>15 Å) interstitial-vacancy pairs calculated within the same supercell. Only a very minor difference in energy was observed for the corresponding close and distant pairs, hence, only energies of well-separated defects are listed in Table 1.

In the split oxygen interstitial defect, a displaced atom forms a dumbbell with a regular atom in such a way that neither atom is on the ideal crystalline site but the two are symmetrically displaced from it. In the hollow interstitial configuration, the displaced atom is located in an available interstitial position. Interstitial defects cause a significant lattice distortion and redistribution of the electronic density.

5. Antisite defects

Along with point defects and Frenkel/Schottky defects, we also studied cation exchange reactions. Energies describing the disorder on the cation sublattice of BSCF are summarized in Table 2. We found that the cation exchange on either the A- or B-sublattices of the ABO_3 perovskite lattice (Eqs. (1) and (2)) requires a small energy for B sites and is weakly exothermic for A sites. From the

Table 1
Single vacancy and vacancy-interstitial pair (Frenkel disorder) formation energies are described in standard Kröger and Vink notations and calculated per defect. Vacancy formation energies in the $Ba_{0.5}Sr_{0.5}Co_{0.75}Fe_{0.25}O_3$ lattice are calculated with respect to the corresponding isolated atoms, as indicated by (g) symbol. V_{Me} stands for the metal vacancy (Me = Ba, Sr, Co, and Fe). Two possible oxygen vacancy configurations were probed, the vacancy placed between two Co atoms, $V_{Co-O-Co}$, and the vacancy placed between one Co and one Fe atom [3,4].

Vacancy	Formation energy (eV)	Frenkel pairs	Interstitial configuration	Formation energy (eV)
(1) $V_{Ba} + Ba_{(g)}$	9.19	$V''_{Ba} + Ba^{\cdot\cdot}_{i}$	Split	6.02
(2) $V_{Sr} + Sr_{(g)}$	9.32	$V''_{Sr} + Sr^{\cdot\cdot}_{i}$	Split	4.49
(3) $V_{Co} + Co_{(g)}$	8.63	$V''''_{Co} + Co^{\cdot\cdot\cdot\cdot}_{i}$	Hollow	1.76
(4) $V_{Fe} + Fe_{(g)}$	9.76	$V''''_{Fe} + Fe^{\cdot\cdot\cdot\cdot}_{i}$	Hollow	2.41
(5) $V_{Co-O-Co} + O_{(g)}$	3.96/1.34[a]	$V^{\cdot\cdot}_{Co-\mathbf{O}-Co} + O''_{i}$	Split	0.75
			Hollow	1.85
(6) $V_{Co-O-Fe} + O_{(g)}$	4.02/1.40[a]	$V^{\cdot\cdot}_{Co-\mathbf{O}-Fe} + O''_{i}$	Split	0.89
			Hollow	1.88

[a] The second energy is calculated with respect to 1/2 free O_2 molecule in the triplet state.

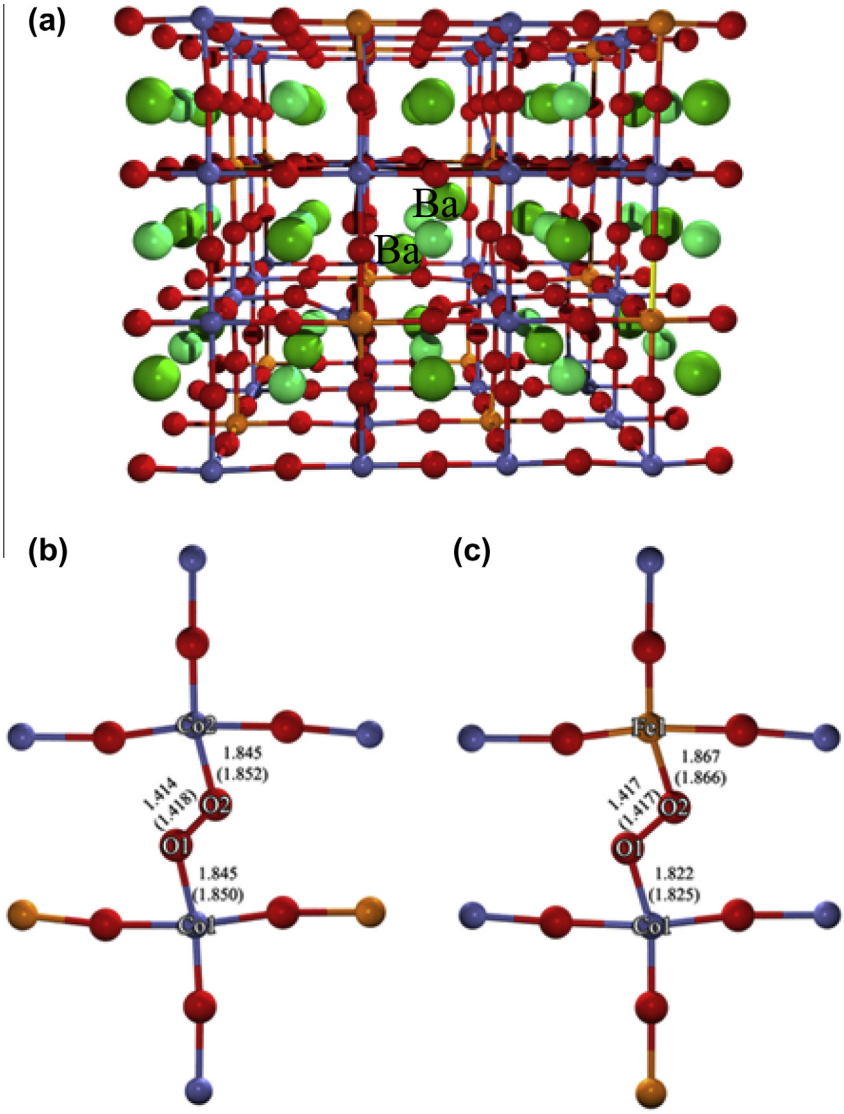

Fig. 2. (a) Ba split interstitial configuration is shown in the 320 atom model supercell of BSCF, (b) and (c) two different configurations of O split interstitial defects. The numbers indicate distances between atoms in a close Frenkel pair (and in a corresponding distant Frenkel pair).

energetic point of view, this indicates that both the A-site metals (Ba and Sr) and the B-site metals (Co and Fe) can be almost randomly dissolved on the respective sublattices; this is in agreement with earlier calculations [13]. This conclusion lends strong support to the high tolerance of the cubic polymorph towards the A-site and B-site compositions suggested based on TEM images and Selected Area Electron Diffraction (SAED) patterns of cubic and hexagonal BSCF [14].

Exchanging one Ba with one Sr in the supercell results in the aggregation of the Sr and Ba perovskite phases, referred to as the cation clustering effect. In a sense, this is a manifestation of the self-segregation process on the cation sublattices.

Furthermore, we established that antisite substitutions, or a pair of defects in which an A metal occupies a B position of the ABO_3 lattice and the corresponding B metal fills the A position, (for example, Sr ↔ Co) are also possible (see (3)–(6) in Table 2). However, as expected, they require a significantly higher energy than the clustering of cations within the same sublattice due to the need for charge compensation, the difference in ionic radii of the A and B atoms, and the different coordination numbers in the

Table 2
Energies of the cation structural disorder on the BSCF lattice. Calculations are performed for a single exchange pair of cations placed in a large 320 atom model supercell, which consists of 64 BSCF formula units.

Ideal lattice site (atom)	Defect site (atom)	Energy (eV)	Comment
(1) A_1(Ba); A_2(Sr)	A_1(Sr); A_2(Ba)	−0.20	Clustering of Ba and Sr in A-sublattice
(2) B_1(Co); B_2(Fe)	B_1(Fe); B_2(Co)	0.08	Clustering of Co and Fe in B-sublattice
(3) A(Ba); B(Co)	A(Co); B(Ba)	6.16	Antisite defect: $Ba_A + Co_B \leftrightarrow Ba_B + Co_A$
(4) A(Ba); B(Fe)	A(Fe); B(Ba)	7.87	Antisite defect: $Ba_A + Fe_B \leftrightarrow Ba_B + Fe_A$
(5) A(Sr); B(Co)	A(Co); B(Sr)	3.79	Antisite defect: $Sr_A + Co_B \leftrightarrow Sr_B + Co_A$
(6) A(Sr); B(Fe)	A(Fe); B(Sr)	5.70	Antisite defect: $Sr_A + Fe_B \leftrightarrow Sr_B + Fe_A$

ideal crystalline lattice. Bearing in mind that the cation diffusion is relatively slow, the antisite defects can be hardly considered as a favorable disorder in BSCF.

6. Summary and conclusions

We presented and discussed the results of first principles calculations of BSCF perovskite solid solutions containing basic point defects (cation and anion vacancies, cation exchange, and antisite defects), as well as structural disorder (Frenkel and Schottky defects). Our DFT modeling reveals that both oxygen Frenkel and Schottky disorders have quite low formation energies and are energetically favorable. The calculated cation exchange energies are very low on both the A- and B-sublattices (Ba ↔ Sr and Co ↔ Fe) of the cubic perovskite structure; this should lead to an easy aggregation of cations with further phase separation. In contrast, antisite defects (A ↔ B exchange) are costly and unlikely to contribute to disorder in these materials. Thus, in general, complex perovskite solid solutions (for example double perovskites discussed here) can accommodate much larger defect disorder than parent ABO_3 perovskites. An analysis of possible BSCF decomposition into different phases or binary oxides is presented in Ref. [15].

Acknowledgements

This research is supported in part by the Latvian National Programme on Materials (VPP IMIS), the European Union COST Program CM1104, and the US National Science Foundation (NSF, Grant CMMI-1132451). Authors thank NSF for its support through TeraGrid resources provided by the Texas Advanced Computing Center (TACC) and the National Center for Supercomputing Applications (NCSA) under Grant No. TG-DMR100021. M.M.K. is grateful to the Office of the Director of NSF for support under the IRD Program. Any appearance of findings, conclusions, or recommendations, expressed in this material are those of the authors and do not necessarily reflect the views of NSF.

References

[1] See, for example E.A. Kotomin, R. Merkle, Yu A. Mastrikov, M.M. Kuklja, J. Maier, Energy conversion—solid oxide fuel cells: first-principles modeling of elementary processes, in: C. Richard, A. Catlow, A.A. Sokol, A. Walsh (Eds.), Computational Approaches to Energy Materials, John Wiley & Sons, The Atrium, Southern Gate, Chichester, West Sussex, PO19 8SQ, United Kingdom, 2013, pp. 149–186.
[2] Yu A. Mastrikov, M.M. Kuklja, E.A. Kotomin, J. Maier, Energy Environ. Sci. 3 (2010) 1544–1550.
[3] E.A. Kotomin, Yu A. Mastrikov, M.M. Kuklja, R. Merkle, A. Roytburd, J. Maier, Solid State Ionics 188 (2011) 1–5.
[4] R. Merkle, Yu A. Mastrikov, E. Kotomin, M.M. Kuklja, J. Maier, J. Electrochem. Soc. 159 (2012) B219–B226.
[5] B.S. Thomas, N.A. Marks, B.D. Begg, Nucl. Instr. Meth. B 254 (2007) 211–218.
[6] G. Kresse, J. Furthmueller, VASP the Guide, University of Vienna, 2003.
[7] NIST Computational Chemistry Comparison and Benchmark Database, 14th ed., Am. Chem. Soc., Washington, 2006.
[8] H.J. Monkhorst, J.D. Pack, Phys. Rev. B 13 (1976) 5188–5192.
[9] G. Henkelman, A. Arnaldsson, H. Jónsson, Comput. Mater. Sci. 36 (2006) 254–360.
[10] Y.F. Zhukovskii, E.A. Kotomin, R.A. Evarestov, D.E. Ellis, Int. J. Quantum. Chem. 107 (14) (2007) 2956–2985.
[11] S. Piskunov, E. Heifets, T. Jacob, E.A. Kotomin, D.E. Ellis, E. Spohr, Phys. Rev. B 78 (2008). 121406 (4 pages).
[12] Y.A. Mastrikov, R. Merkle, E. Heifets, E.A. Kotomin, J. Maier, J. Phys. Chem. C 114 (7) (2010) 3017–3027.
[13] S. Gangopadhayay, T. Inerbaev, A.E. Mansurov, D. Altilio, N. Orlovskaya, Appl. Mater. Interface 1 (2009) 1512–1519.
[14] D.N. Mueller, R.A. De Souza, T.E. Weirich, D. Roehrens, J. Mayer, M. Martin, Phys. Chem. Chem. Phys. 12 (2010) 10320–10328.
[15] M.M. Kuklja, Y.A. Mastrikov, B. Jansang, E.A. Kotomin, J. Phys. Chem. C 116 (2012) 18605–18611. ibid, Solid State Ionics 230 (2013) 21–26.